Orbit Design and Insertion for the JAXA Transformable Spacecraft

By Javier HERNANDO-AYUSO,[1)], Nicola BARESI[2)] and Toshihiro CHUJO[2)]

[1)]*Department of Aeronautics and Astronautics, The University of Tokyo, Tokyo, Japan*

[2)]*Institute of Space and Astronautical Science, Japanese Aerospace Exploration Agency, Sagamihara, Japan*

Detection of possible Earth-impacting asteroids is a crucial task in planetary defense. However, impacts of often undetected small asteroids are not uncommon, as in the case of the Chelyabinsk meteor. A dedicated space-based telescope could vastly improve the last-minute detection of Earth-impacting asteroids, and increase the warning time to several days. One very promising location for such a spacecraft is around a Lagrange point of the Sun-Earth system, as stable observation conditions can be achieved. The solar radiation pressure acceleration can be exploited to obtain perturbed small-amplitude Halo orbits which are seen as circles in the plane of the sky from Earth, avoiding eclipse periods. In order to effectively achieve station-keeping using solar radiation pressure and astronomical observations in a small satellite, the concept of the *"Transformable Spacecraft"* was proposed in ISAS/JAXA in late 2017, which is characterized by a reconfigurable structure. In this paper, the orbit design for the Transformable Spacecraft is presented, and the effect of the design parameters is analyzed. Additionally, the low-energy insertion from Earth to the actual orbit with a Moon flyby is presented using two different models. The first one is the Circular Restricted Three Body Problem considering the Sun and Earth describing a circular orbit, and including the Moon's gravitational influence only during the flyby. We also study the transfer in the context of the Bicircular Restricted Four Body Problem for a more precise result of the necessary Delta-V at departure from Low Earth Orbit.

Key Words: Transformable Spacecraft, Halo Orbit, Solar Radiation Pressure, Solar Sail

1. Introduction

Detection of possible Earth-impacting asteroids is a crucial task in planetary defense. Extensive monitoring is routinely performed for known asteroids by ground-based telescopes and radars. However, impacts of often undetected small asteroids are not uncommon, as in the case of the Chelyabinsk meteor or the asteroid 2018LA which reentered in the skies of southern Africa on early June 2018. In some cases, an Earth-impacting asteroid can be detected from surface on its final approach, but the time to impact is often short and the uncertainty is high. A dedicated space-based telescope could vastly improve the last-minute detection of Earth-impacting asteroids, and increase the warning time to several days. Furthermore, this telescope could also survey resources in potential asteroid mining candidates to support future activities. To do so, the spacecraft must be able to switch between wide-field surveys for Earth-impact monitoring and narrow-field observations for resource surveys. For both mission objectives, it is desired to keep the spacecraft close to a Lagrange point for steady observation conditions. Moreover, asteroid monitoring requires infrared detectors, which need cooling. This calls for a stable and favorable thermal environment, which can be achieved at the L2 point of the Sun-Earth L2 system (SEL2) because the illumination conditions does not change significantly with time and the radiation from the Sun and the Earth comes from the same direction.

Classically employed Halo orbits have drawbacks such as eclipses and relatively large amplitudes. Figure 1 shows the family of planar Lyapunov orbits, and the north halo orbits which bifurcate from the Lyapunov planar. In order to avoid eclipses, the magnitude of the orbit amplitude must be on the order of 10^6km, which would cause large variations in the observation geometry during the orbit. Tanaka et al. proposed to exploit the solar radiation pressure acceleration to achieve perturbed small-amplitude Halo orbits which are seen almost as circles in the plane of the sky from Earth, avoiding being eclipsed by the Earth [1)] . Using this technique, the amplitude of the orbit can be chosen on the order of $\simeq 10^4$ km (see Fig. 2), which is two orders of magnitude below the planar Lyapunov and the north-south halo orbit families mentioned above.

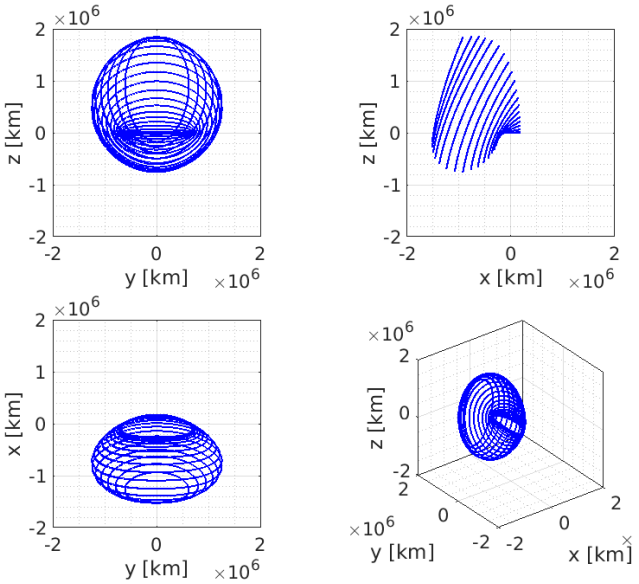

Fig. 1. Traditional Halo orbits families (Planar and North). The orbit amplitude is on the order of 10^6 km.

JAXA is working in an innovative mission concept of a telescope mission that exploits the points mentioned above. [2)] Another novel contribution of the proposal is that the space-

This note was presented at the 28th JAXA Workshop on Astrodynamics and Flight Mechanics at Sagamihara (Japan), with manuscript number B-26

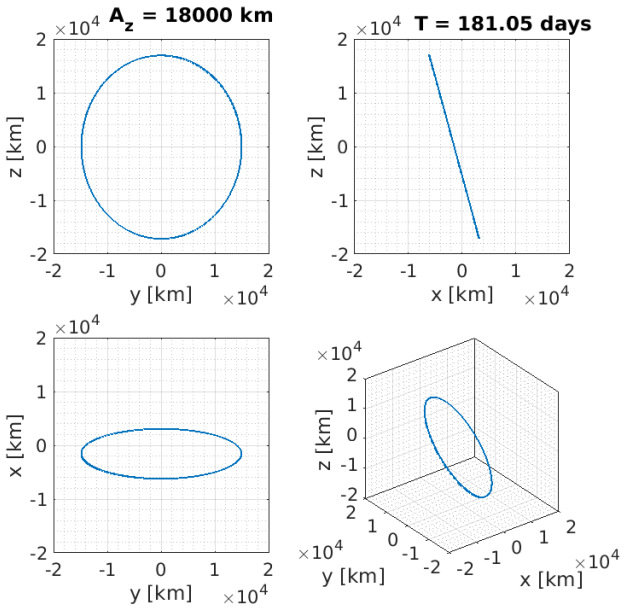

Fig. 2. SRP-assisted small-amplitude quasi-circular halo orbits (Tanaka et. al. 2006). The orbit amplitude is on the order of 10^4 km.

craft is composed of plates connected by hinges and actuators, which enables fuel-free attitude control by exploiting the non-holonomic dynamics that characterize the relative rotation of the plates. [3] The state in a non-holonomic system depends on the path followed to reach it. Thus, by changing the order of the rotations of the plates, it is possible to obtain a different attitude of the spacecraft with respect to an inertial frame, even if the initial and final configuration of the spacecraft is identical.

Additionally, the capability to change its shape allows the spacecraft to switch between different observation modes and to assume a compact shape on the launch vehicle. The temporary name for this spacecraft is *Transformable spacecraft*, because it can transform its shape to achieve all the mission objectives.

The current design considers 19 plates. Each plate has a surface area of 1 m^2 and a mean mass of 10 kg, including hinges and actuators. Six of these plates are covered by solar arrays, ten are covered by MLI, two have photo-detectors and the last plate has a mirror with MLI on its back. Figure 3 shows the plates of the spacecraft and their connections. MLI is shown in yellow, solar arrays in black, the mirror in white, the photo-detectors in red, and the connection between the plates are shown in blue. With this configuration, the spacecraft can switch between different modes, as shown in Fig. 4

In this paper, we first present the orbit design for the transformable spacecraft, and then evaluate the impact of the spacecraft and control law parameters in the orbit. Finally, we present the orbit insertion into the SRP-assisted halo orbit with a low-energy transfer exploiting the natural dynamics and a gravity assist at the Moon.

2. Circular Restricted 3 Body Problem

We employ the Circular Restricted 3 Body Problem (CR3BP) of the Sun-Earth (SE) system to design the orbit of the Transformable spacecraft. In the frame of the CR3BP, the spacecraft

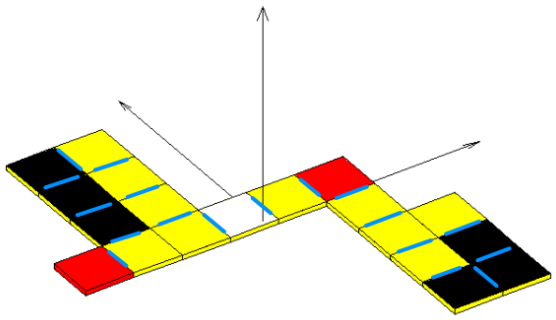

Fig. 3. Transformable spacecraft composed of 19 plates connected by hinges and actuators.

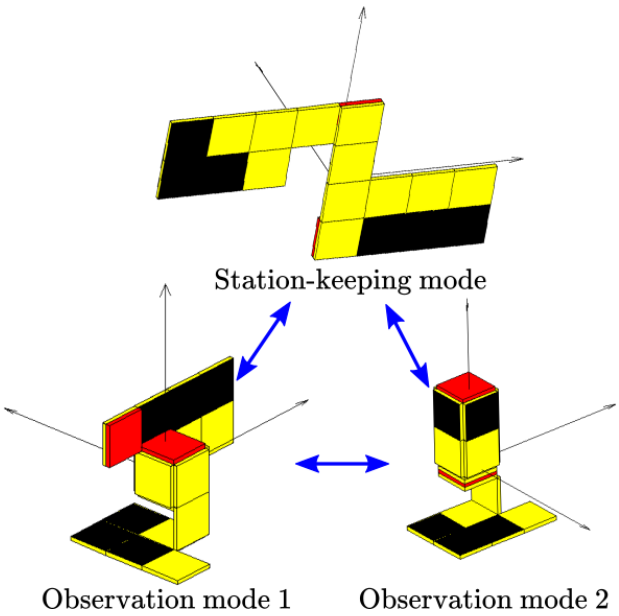

Fig. 4. Different configuration modes of the Transformable spacecraft.

is considered to have negligible mass compared to two massive bodies which describe circular orbits around the system barycenter. [4] We define the synodic frame $\langle x, y, z\rangle$ centered at the Lagrange Point L2. This frame rotates around the z axis solidary with the Earth and the Sun, and the x axis is oriented in the Sun-Earth direction. The coordinates of Earth's center in this frame become $(-\gamma, 0, 0)^\top$, where γ is given by the only real root of [4]

$$\gamma^5 + (3-\mu)\gamma^4 + (3-2\mu)\gamma^3 - \mu\gamma^2 - 2\mu\gamma - \mu = 0, \quad (1)$$

$$\mu = \frac{M_\oplus}{M_\oplus + M_\odot} \quad (2)$$

where $\oplus$ stands for the Earth and $\odot$ stands for the Sun. For the Sun-Earth system, $\mu \simeq 3.0395 \times 10^{-6}$ and $\gamma \simeq 0.01008$. The geometry of the CR3BP is shown in Fig. 5

The equations of motion of the CR3BP are:

$$\ddot{x} - 2\dot{y} = -\frac{\partial U}{\partial x} + a_x, \quad (3a)$$

$$\ddot{y} + 2\dot{x} = -\frac{\partial U}{\partial u} + a_y, \quad (3b)$$

$$\ddot{z} = -\frac{\partial U}{\partial z} + a_z, \quad (3c)$$

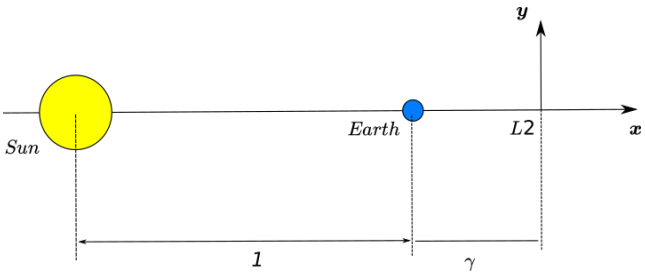

Fig. 5. Geometry of the CR3BP

where U is the effective potential

$$U = -\frac{1}{2}\left((x+1-\mu+\gamma)^2+y^2\right) - \frac{1-\mu}{r_\odot} - \frac{\mu}{r_\oplus}, \quad (4)$$

and where the distances to the Sun and the Earth are

$$r_\odot = \sqrt{(x+1+\gamma)^2+y^2+z^2} \quad (5)$$

and

$$r_\oplus = \sqrt{(x+\gamma)^2+y^2+z^2}, \quad (6)$$

respectively. Finally, we consider a perturbing acceleration acting on the spacecraft $\boldsymbol{a} = \left(a_x, a_y, a_z\right)^\top$.

2.1. Solar radiation Pressure perturbation

We model the effect of the solar radiation pressure (SRP) perturbing acceleration considering the effects of diffusion, specular reflection and absorption over a flat plate. The perturbing acceleration takes the form

$$\boldsymbol{a}_{\mathrm{SRP}} = -\frac{PS}{m}(\boldsymbol{s}\cdot\boldsymbol{n})\left\{\left(1-C_{\mathrm{spe}}\right)\boldsymbol{s} + \left(\frac{2}{3}C_{\mathrm{dif}} + 2(\boldsymbol{s}\cdot\boldsymbol{n})C_{\mathrm{spe}}\right)\boldsymbol{n}\right\}, \quad (7)$$

where $P = 4.47\times10^{-6}$ Pa is the solar radiation pressure at 1 au, and S and m are the spacecraft area and mass, respectively. The optical properties of the surface are defined as follows. C_{spe} is the specular reflection coefficient, C_{dif} is diffusive reflection coefficient and we considered $C_{\mathrm{abs}} = 1 - C_{\mathrm{spe}} - C_{\mathrm{dif}}$ as the absorption coefficient. Finally, $\boldsymbol{s}$ is the Sun vector and $\boldsymbol{n}$ is the surface normal. To give the orientation of the surface normal, we employ two angles: ψ and φ. The angle ψ is a rotation from the $-x$ direction around an axis perpendicular to the ecliptic plane, while φ is a subsequent rotation outside the orbital plane and positive towards the Earth orbital angular momentum. These angles are sketched in Fig. 6, and they allow to write the normal vector coordinates in the rotating frame as

$$\boldsymbol{n} = (-\cos\varphi\cos\psi, -\cos\varphi\sin\psi, \sin\varphi)^\top. \quad (8)$$

For the nominal orbit, we consider the station-keeping mode shown in Fig. (4), in which 6 solar arrays and 11 MLI plates are exposed to the Sun. This gives a surface S equal to 17m^2. The mass of the spacecraft is equal to 190 kg. The optical properties of each type of panel are summarized in Table 1.

Table 1. Optical properties.

	C_{spe}	C_{dif}	C_{abs}
MLI	0.375	0.255	0.370
Solar cells	0.086	0.060	0.854
Perfect mirror	1	0	0

Fig. 6. Angles for the flat-plate spacecraft orientation.

2.2. Control law for the linearized system

After subsituting Eq. (7) into Eq. (3), the equations of motion can be linearized around the L2 point as [1)]

$$\ddot{x} - 2\dot{y} - (1+2c_2)\,x = k_1 \quad (9a)$$
$$\ddot{y} + 2\dot{x} + (c_2-1)\,y = k_2\psi \quad (9b)$$
$$\ddot{z} + c_2 z = -k_2\varphi \quad (9c)$$

with

$$c_2 = \frac{\mu}{\gamma^3} + \frac{1-\mu}{(1-\gamma)^3} \simeq 3.9405645$$
$$k_1 = \frac{PS}{m}\left(C_{\mathrm{abs}} + \frac{5}{3}C_{\mathrm{dif}} + 2C_{\mathrm{spe}}\right),$$
$$k_2 = \frac{PS}{m}\left(\frac{2}{3}C_{\mathrm{dif}} + 2C_{\mathrm{spe}}\right).$$

Equation (9) admit a solution of the type:

$$x = -\frac{A_z}{\alpha}\cos(\omega t) + x_e, \quad (10a)$$
$$y = A_z\sin(\omega t), \quad (10b)$$
$$z = \pm A_z\cos(\omega t), \quad (10c)$$

and by substituting into Eq. (9), the following necessary conditions are found: [1)]

$$x_e = -\frac{k_1}{1+2c_2}, \quad (11a)$$
$$\alpha = \frac{\omega^2+1+2c_2}{2\omega}, \quad (11b)$$
$$\psi = \left(c_2 - \omega^2 + 2\frac{\omega}{\alpha} - 1\right)\frac{A_z}{k_2}\sin(\omega t), \quad (11c)$$
$$\varphi = \mp\left(c_2-\omega^2\right)\frac{A_z}{k_2}\cos(\omega t). \quad (11d)$$

Under linear dynamics, the proposed orbit is circular in the plane of the sky as seen from Earth, and its amplitude can be freely chosen. However, the amplitude should be greater than 13460 km to avoid eclipses, as sketched in Fig. 7. For the nominal orbit, we will add a margin to account for nonlinearities and operational margins and will use $A_z = 18000$ km.

The frequency of the orbit ω is another free parameter, but must be chosen in the vicinity of $\omega = 2$ so the control angles ψ and φ remain small as can be seen in Fig. 8. If ω is chosen far from this value, the control angles may become greater

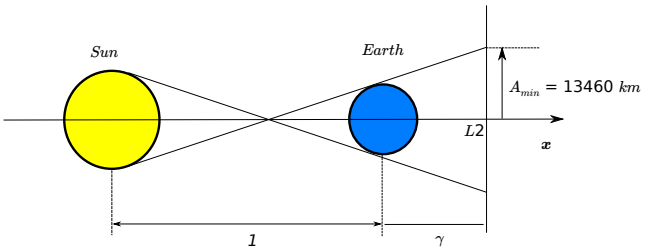

Fig. 7. Minimum amplitude for eclipse avoidance.

than 90 deg, which would be physically unfeasible. For specific values of ω, φ or ψ vanishes:

$$\omega = \sqrt{c_2} \simeq 1.985, \quad \varphi = 0 \tag{12a}$$

$$\omega = \sqrt{\frac{1}{2}\sqrt{c_2(9c_2-8)} - \frac{c_2}{2} + 1} \simeq 2.057, \quad \psi = 0 \tag{12b}$$

Moreover, there is a value of ω that minimizes the maximum amplitude of the control angles. This happens when the amplitude in Eqs. (11c, 11d) coincides, which yields

$$\omega = \frac{1}{2}\sqrt{\sqrt{(2c_2-1)(18c_2+7)} - 2c_2 + 1} \simeq 2.0172. \tag{13}$$

In order to reduce nonlinear effects in the next section, we will employ $\omega = 2.0172$ as the orbital frequency. With this choice, the orbital period becomes around 181.05 days.

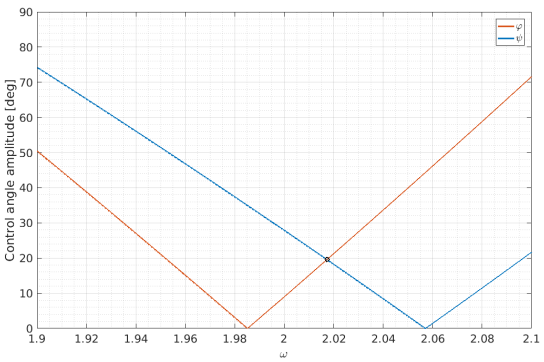

Fig. 8. Amplitude of the control angles as a function of the control frequency.

2.3. Periodic orbit with nonlinear dynamics

When the fully nonlinear dynamics governed by Eq. 3 are considered, the solution proposed for the linear case (Eq. 10) will fail to describe periodic orbits. In general, it is possible to adjust the initial state to generate periodic orbits. We employ a Newton-Raphson method using the linear solution as initial guess $\boldsymbol{x}_0$, and numerically calculate the initial conditions that will satisfy the periodicity condition $\boldsymbol{F}(\boldsymbol{x}_0)$ after a period T:

$$\boldsymbol{F}(\boldsymbol{x}_0) = \boldsymbol{x}(T) - \boldsymbol{x}_0 = \boldsymbol{0}. \tag{14}$$

The gradient of the periodicity condition is given by

$$\frac{\partial \boldsymbol{F}}{\partial \boldsymbol{x}_0} = \boldsymbol{\phi}(T) - \boldsymbol{I}, \tag{15}$$

where $\boldsymbol{\phi}(T)$ is the state transition matrix after one period, also called the monodromy matrix. Using Newton-Raphson method, the update in the initial conditions is given by

$$\delta \boldsymbol{x}_0 = -\left(\frac{\partial \boldsymbol{F}}{\partial \boldsymbol{x}_0}\right)^{-1} \boldsymbol{F}(\boldsymbol{x}_0). \tag{16}$$

We update the initial conditions until the periodicity condition is satisfied up to some tolerance, and the variation in $\delta \boldsymbol{x}_0$ is small enough.

We described above a single-shooting algorithm: we modify the initial condition to adjust the state after one orbital period. To improve convergence of the Newton-Raphson method, it is possible to divide the trajectory into multiple arcs and impose continuity conditions between them, constructing a multiple-shooting method. The multiple-shooting method can improve the convergence to the periodic orbit since the unstable nature of the dynamics around L2 has less time to act on the trajectory in each arc. A detailed description of a multiple-shooting algorithm for periodic orbit calculation can be found in [5].

3. Sensitivity analysis

In this section we explore the sensitivity of the nominal orbit with respect of several parameters that affect the size and shape of the period orbits that can be achieved.

3.1. Effect of the frequency of the control law

The frequency of the control law has a direct efect on the period of the orbit, as we always employ orbits which are in a $1:1$ resonance with the control law. We introduced previously how the amplitude of the control angles change with the frequency (see Fig. 8). A larger control angle will yield a larger difference between the periodic orbits constructed in the linear and the nonlinear systems. This can be observed in Fig. 9, where we present periodic orbits for different values of ω. For values of ω smaller than the nominal, the orbit amplitude outside the ecliptic plane increases, and the amplitude in the y direction decreases slightly. For larger values of ω, the orbit becomes smaller until it is eventually inside the eclipse limit.

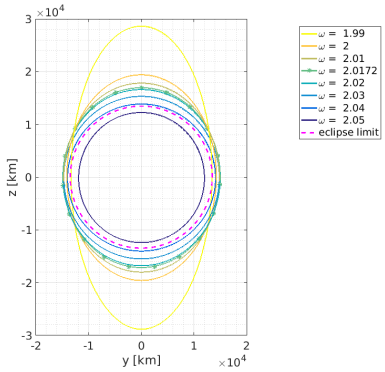

Fig. 9. Family of orbits changing the orbit frequency.

3.2. Effect of the amplitude of the control law

The amplitude A_z in the control law (see Eqs. (11c, 11d)) is equivalent to the orbit amplitude only in the linear case. When considering nonlinear dynamics, the amplitude in the y and z directions becomes different in the general case. Figure 10 shows the orbit amplitudes as a function of the amplitude of the control. We have included as a reference the nominal orbit as an asterisk, and the prediction of the linear system with a black dashed line. It is interesting to note that the amplitude of the control cannot be made arbitrarily large: for some value of A_z the control saturates and the orbit amplitude decreases. This is

associated to a saturation of the maximum SRP force that a flat surface can provide when changing the attitude.

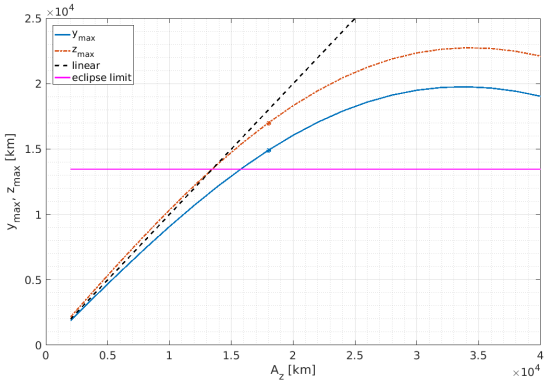

Fig. 10. Effect of changing the orbit amplitude A_z.

Figure 11 shows the family of orbits that can be obtained by changing the control amplitude. The saturation effect of the control is also present in this figure. For higher values of A_z, the orbits grow larger and larger until they reach a maximum, becoming smaller for increasing values of A_z. Additionally, for very small values of A_z the orbits are closer to circles. This is to be expected, as the linear approximation holds for sufficiently small orbits.

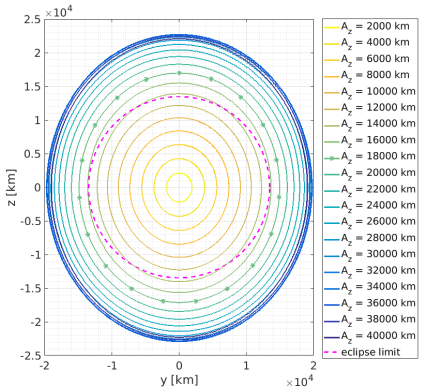

Fig. 11. Family of orbits changing the control amplitude A_z.

3.3. Effect of the number of panels

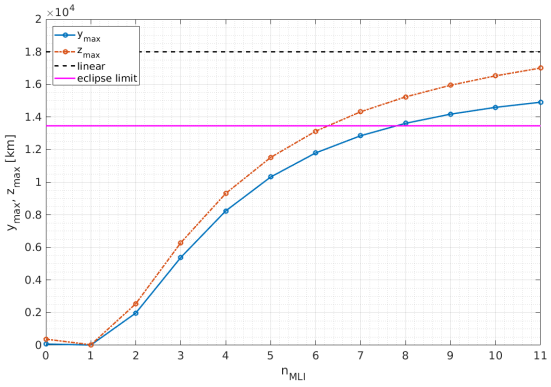

Fig. 12. Effect of using only a number of MLI panels.

If the spacecraft fails to implement the attitude control law, it will start to depart from the periodic orbit owing to the saddle structure of the dynamics around SEL2. It is interesting to the

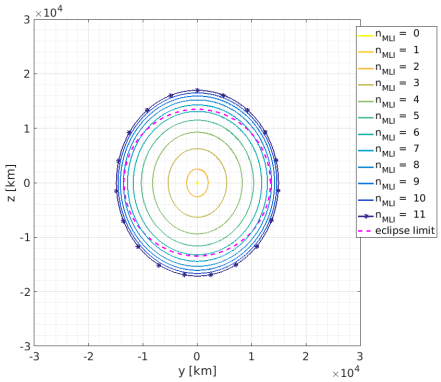

Fig. 13. Family of orbits using only a number of MLI panels.

performance of the system when only a fraction of the panels are used in the nominal control law, so the panels kept as a backup can offer an increment in SRP force to recover and come back to the nominal orbit. The orbit amplitude as a function of the number of MLI panels used is shown in Fig. 12. For reference, the nominal orbit is using 11 MLI panels. It becomes clear that in order to avoid eclipses, the number of panels must be at least 8. A similar conclusion can be drawn from the y–z plot of these periodic orbits, shown in Fig. 13.

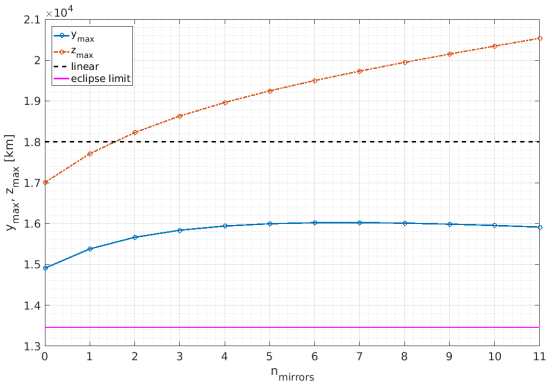

Fig. 14. Effect of adding perfect mirrors.

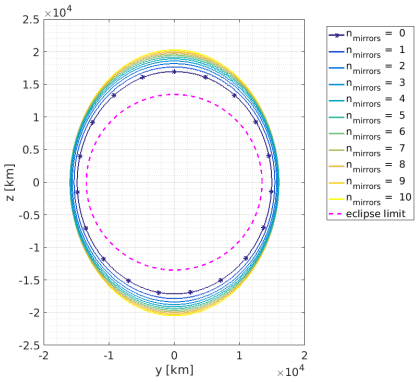

Fig. 15. Family of orbits adding perfect mirrors.

Another possibility that the project team is considering is adding additional perfect mirrors to support the orbit-reinsertion operations. The effect of adding additional perfect mirrors with no mass increase is shown in Figs. 14 and 15. Adding perfect mirrors is an effective way to increase the orbit amplitude outside the ecliptic plane, but a smaller effect is

obtained in the y direction, which shows saturation for about 6 additional mirrors. Further work is needed in this direction, as an increased number of panels will likely have an impact on the spacecraft mass.

3.4. Effect of the surface-to-mass ratio

The surface-to-mass ratio plays a key role in the periodic orbits that can be achieved using the control law of Eqs. (11c, 11d). This control law was designed for solar sails, which feature a large surface area with a small mass and can effectively exploit the SRP acceleration. For instance, IKAROS had a surface-to-mass ratio of approximately $0.6\,\mathrm{m}^2/\mathrm{kg}$. However, the nominal configuration for the Transformable spacecraft has a ratio equal to $0.089474\,\mathrm{m}^2/\mathrm{kg}$, and the effectiveness of the control law will be smaller compared to a solar sail. In this subsection, we explore how the amplitude of the periodic orbit changes as a function of the surface-to-mass ratio.

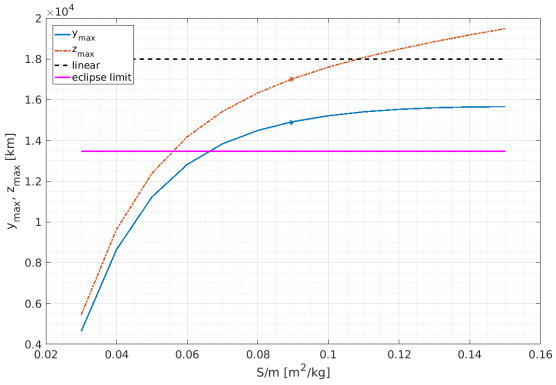

Fig. 16. Effect of changing the surface-to-mass ratio S/m.

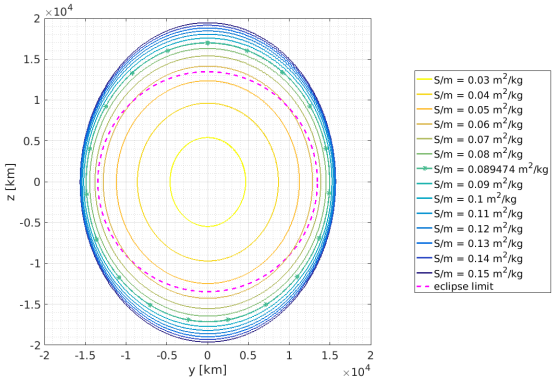

Fig. 17. Family of orbits changing the surface-to-mass ratio S/m.

Figure 16 shows the maximum amplitude of the family of periodic orbits achieved, with the nominal value indicated by a marker. Increasing the surface-to-mass ratio seems to be an effective way of increasing the out-of-plane amplitude, while it has less effect on the in-plane component. The family of periodic orbits is shown in Fig. 17.

4. Orbit insertion

In this section we explore the insertion into the periodic orbit after launch from Earth.

It is possible to transfer from Earth to SEL2 in a relatively short time using chemical propulsion for maneuvers at arrival in SEL2. The transfer duration is between 30 and 120 days, with a Δv at SEL2 arrival between 0.1 and 0.7 km/s. This option imposes requirements on the spacecraft structure and the mass budget that were considered to be too strict by the project team. Hence, the option of a low energy transfer with a lunar gravity assist is considered here at the expense of a longer time of flight. First, we consider the consider the natural dynamics of the CR3BP to obtain orbits that arrive in SEL2 and include an instantaneous flyby by the Moon. Then, we employ the Bicircular Restricted 4 Body Problem (BR4BP) to better account for the Moon's gravitational effect on all the legs of the trajectory to obtain a more precise result.

4.1. Transfer in the CR3BP

The transfer using the model of the CR3BP is divided in three legs: Earth departure, instantaneous Moon gravity assist and periodic orbit insertion following the stable manifold around SEL2. The design of this phases is best performed in reverse order, starting at the periodic orbit and going backwards on time.

4.1.1. Stable Manifold

The saddle-point nature of L2 implies that a stable and a unstable direction exist in this region of space. Associated to each periodic orbit, stable and unstable manifolds exist such that when the spacecraft is on them, it approaches or gets away from the periodic orbit following an exponential function of time. The stable manifold is especially useful for the orbit insertion, because if the spacecraft is inserted into the stable manifold, it will eventually lead to the periodic orbit. Here, we only consider the gravitational forces of the Sun and the Earth.

To calculate the stable manifold, we follow the next steps. First, we sample N points from the periodic orbit to populate the manifold. For each of them, we calculate their monodromy matrix and solve for their eigenvalues and eigenvectors. The eigenvector associated to eigenvalue smaller than unity is tangent to the stable manifold. To calculate the trajectory on the stable manifold, we add a shift $\epsilon = 10^{-6}$ on the the mentioned eigenvector and propagate backwards in time. Figure 18 shows the local structure of the stable manifold in the proximity of the periodic orbit. Note that since an eigenvalue is determined up to its sign, a part of the stable manifold connects to the proximity of Earth and the other part leads to deep space. Figure 19

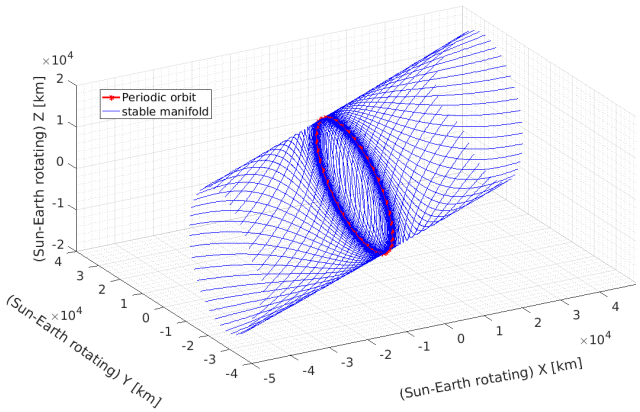

Fig. 18. Stable manifold in the proximity of the periodic orbit.

shows the connection of the stable manifold with the Moon's orbit, shown as a circle around the Earth, which is located about

15×10^5 km from SEL2 in the direction of the Sun.

Among all the trajectories in the stable manifold, we pick the one that has the smallest out-of-plane component when crossing the Moon's orbit. This result is shown in Fig. 19.

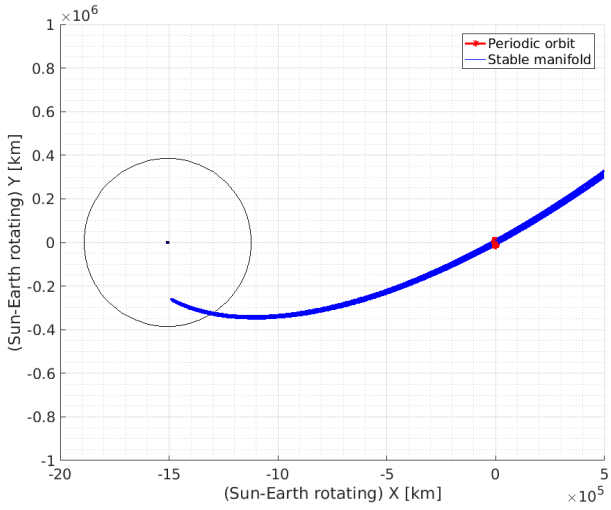

Fig. 19. Connection of the stable manifold with the Moon's orbit.

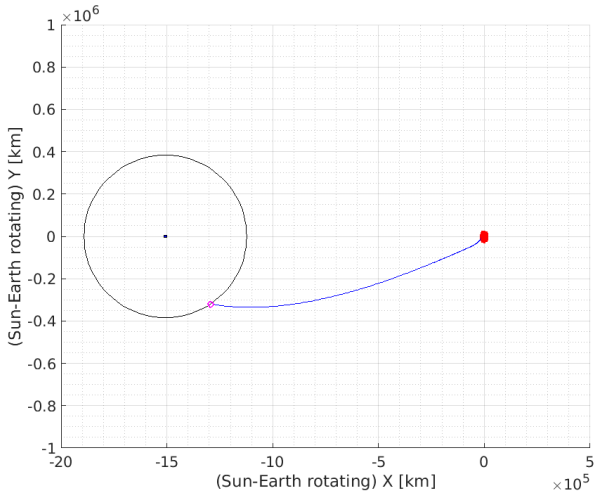

Fig. 20. Intersection of the stable Manifold and the Moon's orbit.

4.1.2. Instantaneous Lunar Gravity Assist

We consider the gravitational effect of the Moon only when the spacecraft is moving in its proximity. For simplicity, we model this motion as an instantaneous flyby, which results in a rotation of the Selenocentric velocity around the direction of the Selenocentric angular momentum vector by an angle $\delta(r_p)$:

$$\delta = 2\sin^{-1}\left(\frac{1}{1+\frac{r_p v_\infty^2}{\mu_{\mathfrak{D}}}}\right),$$

where $\mu_{\mathfrak{D}} \simeq 4.9 \times 10^3\,\mathrm{km}^3/\mathrm{s}^2$ is the Moon's gravitational constant, r_p is the perilune distance, and v_∞ is the hyperbolic excess velocity of the selenocentric orbit. For this particular application, $v_\infty = 0.815$ km/s.

There are two different family of solutions of the instantaneous flyby as a function of the perilune distance. The first one is for a flyby on the leading-side of the Moon, in which the incoming orbit has a larger velocity than the Moon. The second one is for a flyby on the trailing-side, characterized by a lower velocity of the incoming orbit with respect to the Moon. Figure 21 shows these families of solution, where the cyan trajectories correspond to trailing-side flybys, and the yellow curves are for leading-side flybys.

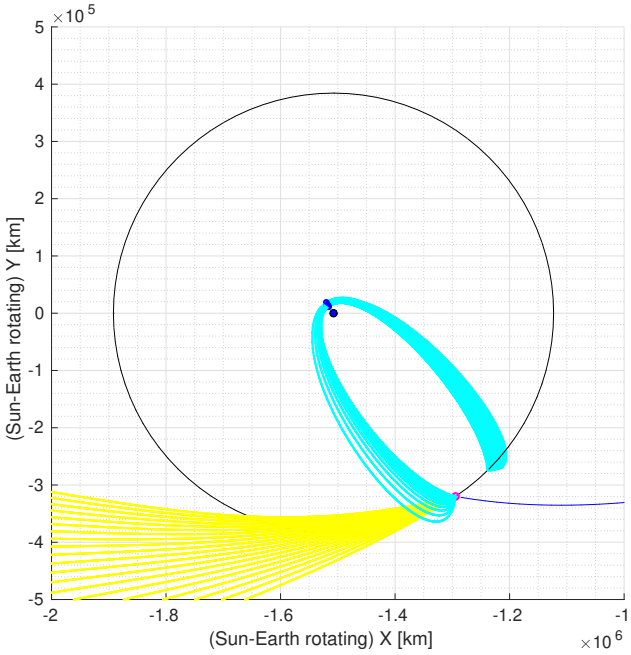

Fig. 21. Families of lunar flybys for different perilune distances.

Only the trailing-side family connects with the vicinity of the Earth. For this family of solutions, Fig. 22 shows the necessary deflection angle and the corresponding perigee altitude, which has a minimum of about 8000 km. This corresponds to a Moon flyby altitude of about 2500 km and a deflection angle of approximately 78 deg.

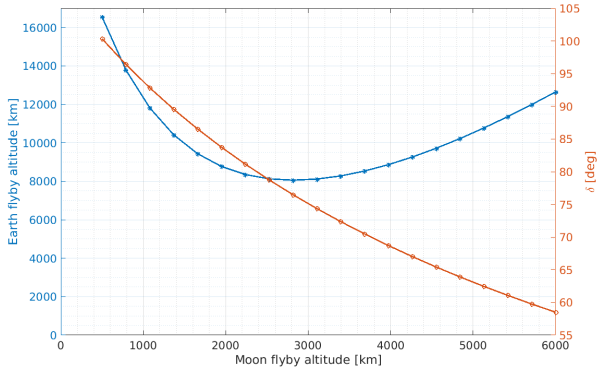

Fig. 22. Earth flyby altitude and Moon flyby velocity deflection angle for the trailing side Moon flybys as a function of the Moon flyby altitude.

The transfer trajectory with all its legs is shown in Fig. 23. This trajectory is characterized by an initial distance from earth of 1.44×10^4 km with a velocity of 7.34 km/s, which yields a value of the characteristic energy $C_3 = -1.38\,\mathrm{km}^2/\mathrm{s}^2$. The total time of flight is 233.3 days, of which 5.1 of them are spent on the Earth-Moon transfer.

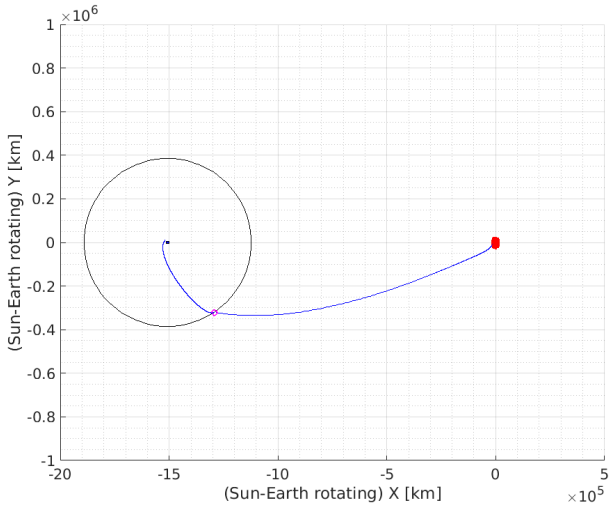

Fig. 23. Transfer using the model of the CR3BP and an instantaneous lunar gravity assist.

4.2. Transfer in the BR4BP

In the Bicircular Restricted 4 Body Problem (BR4BP), we consider that the Moon and the Earth describe circular orbits around the Moon-Earth barycenter, and that this barycenter and the Sun follow circular orbits around the system barycenter.

To calculate the transfer trajectory in this model, we use the same initial condition as in the calculation of the CR3BP manifold. We perform a line search on the Moon phase to minimize the C_3 value of the trajectory that connects with the low Earth orbit region.

Numeric optimization of the trajectory using a grid-search method yields a trajectory with time of flight of 197.8 days and $C_3 = -2.11\,\mathrm{km}^2/\mathrm{s}^2$. The perigee distance at departure is equal to 8748.5 km, and the Moon flyby altitude equal to 2130 km. The optimal trajectory is shown in Fig. 24.

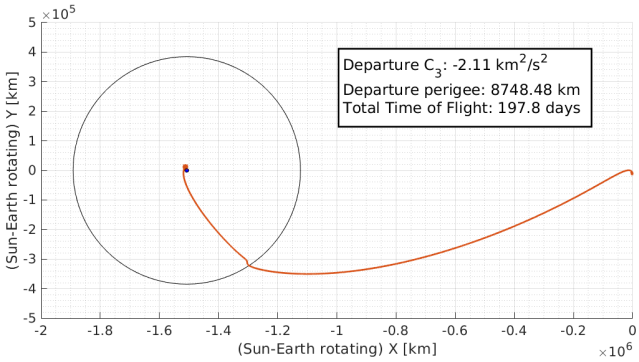

Fig. 24. Transfer using the model of the BR4BP.

5. Conclusions

In the first half of this paper, we presented the design of the orbit of the Transformable spacecraft under study at ISAS/JAXA. We revisited the results by Tanaka et al. [1)] and applied them to this spacecraft. We showed how the solar radiation pressure acceleration can be exploited to obtain low-amplitude, quasi-circular orbits which are free of eclipses, which is key for this spacecraft in order to have a stable power and thermal environment. Furthermore, we studied the effect of the control law and spacecraft parameters on the nominal orbit.

In the second half of the paper, we studied the insertion into the periodic orbit using low-energy transfers, exploiting natural dynamics and a Lunar flyby. We presented results obtained in the Circular Restricted 3 Body Problem and an instantaneous Moon flyby, and compared them to the results yielded in the Bicircular Restricted 4 Body Problem.

Acknowledgments

The authors are indebted to the “Transformable Spacecraft” team for their contributions in the preliminary mission design, and to Keita Tanaka for his constructive comments on constructing circular small Halo orbits following his approach.

The Ministry of Education, Culture, Sports, Science and Technology (MEXT) of the Japanese government supported Javier Hernando-Ayuso under its program of scholarships for graduate school students.

Nicola Baresi acknowledges the support of the Japan Society of Promotion of Science (JSPS) for this research.

References

1) Tanaka, K. and Kawaguchi, J.: Small-amplitude Periodic Orbit around Sun-Earth L1/L2 Controlled by Solar Radiation Pressure, *Transactions of the Japan Society for Aeronautical and Space Sciences*, **59(1)** (2016), pp. 33–42.
2) Chujo, T., Sugawara, Y., Sato, Y., Otsuki, M., Ohashi, K., Kubo, Y., Hernando-Ayuso, J., Matsumoto, J. and Kawaguchi, J.: Concept of transformable spacecraft with variable structure applicable to nonholonomic attitude control and mission overview, *28th Workshop on JAXA Astrodynamics and Flight Mechanics*, B-24, Sagamihara, Japan, 2018.
3) Ohashi, K., Chujo, T. and Kawaguchi, J.: Motion Planning in Attitude Maneuver Using Non Holonomic Turns for a Transformable Spacecraft, *28th Workshop on JAXA Astrodynamics and Flight Mechanics*, B-25, Sagamihara, Japan, 2018.
4) Koon, W. S., Lo, M. W., Marsden, J. E. and Ross, S. D.: *Dynamical systems, the three-body problem and space mission design*, Marsden Books, 2011.
5) Ascher, U. M., Mattheij, R. M. and Russell, R. D.: *Numerical solution of boundary value problems for ordinary differential equations*, volume 13, Siam, 1994, pp. 145-155.